Cellular/Molecular

Presynaptic Short-Term Plasticity Persists in the Absence of PKC Phosphorylation of Munc18-1

Chih-Chieh Wang,[1] Christopher Weyrer,[1,2] Diasynou Fioravante,[1] Pascal S. Kaeser,[1] and Wade G. Regehr[1]
[1]Department of Neurobiology, Harvard Medical School, Boston, Massachusetts 02115, and [2]Department of Physiology, Development, and Neuroscience, University of Cambridge, Cambridge CB2 3EG, United Kingdom

Post-tetanic potentiation (PTP) is a form of short-term plasticity that lasts for tens of seconds following a burst of presynaptic activity. It has been proposed that PTP arises from protein kinase C (PKC) phosphorylation of Munc18-1, an SM (Sec1/Munc-18 like) family protein that is essential for release. To test this model, we made a knock-in mouse in which all Munc18-1 PKC phosphorylation sites were eliminated through serine-to-alanine point mutations (Munc18-1SA mice), and we studied mice of either sex. The expression of Munc18-1 was not altered in Munc18-1SA mice, and there were no obvious behavioral phenotypes. At the hippocampal CA3-to-CA1 synapse and the granule cell parallel fiber (PF)-to-Purkinje cell (PC) synapse, basal transmission was largely normal except for small decreases in paired-pulse facilitation that are consistent with a slight elevation in release probability. Phorbol esters that mimic the activation of PKC by diacylglycerol still increased synaptic transmission in Munc18-1SA mice. In Munc18-1SA mice, 70% of PTP remained at CA3-to-CA1 synapses, and the amplitude of PTP was not reduced at PF-to-PC synapses. These findings indicate that at both CA3-to-CA1 and PF-to-PC synapses, phorbol esters and PTP enhance synaptic transmission primarily by mechanisms that are independent of PKC phosphorylation of Munc18-1.

Key words: **Munc18-1; PKC; plasticity; post-tetanic potentiation; synapse**

Significance Statement

A leading mechanism for a prevalent form of short-term plasticity, post-tetanic potentiation (PTP), involves protein kinase C (PKC) phosphorylation of Munc18-1. This study tests this mechanism by creating a knock-in mouse in which Munc18-1 is replaced by a mutated form of Munc18-1 that cannot be phosphorylated. The main finding is that most PTP at hippocampal CA3-to-CA1 synapses or at cerebellar granule cell-to-Purkinje cell synapses does not rely on PKC phosphorylation of Munc18-1. Thus, mechanisms independent of PKC phosphorylation of Munc18-1 are important mediators of PTP.

Introduction

A brief burst of presynaptic activity transiently increases synaptic strength for tens of seconds at many types of synapses in a phenomenon known as post-tetanic potentiation (PTP; Zucker and Regehr, 2002). It has been proposed that PTP contributes to short-term memory (Zucker and Regehr, 2002; Vyleta et al., 2016; Vandael et al., 2020). Clarifying the mechanism of PTP is important in its own right and could lead to means of selectively eliminating PTP to provide insight into its functional roles.

One of the most promising mechanisms for PTP is that calcium activates protein kinase C (PKC) that in turn phosphorylates Munc18-1 to increase neurotransmitter release (Brager et al., 2003; Wierda et al., 2007; Fioravante et al., 2011; Genç et al., 2014). Munc18-1 plays an essential role in neurotransmitter release. The current working model is that Munc18-1 initially binds the close conformation of syntaxin-1, and then, along with Munc13-1, opens syntaxin-1, leading to partial SNARE complex assembly and the formation of the readily releasable pool (Dulubova et al., 1999; Toonen et al., 2005; Arunachalam et al., 2008; Dawidowski and Cafiso, 2013, 2016; Imig et al., 2014; Rizo, 2018). Deletion of Munc18-1 eliminates both spontaneous and evoked neurotransmitter release (Verhage et al., 2000; Han et al., 2010). It has been proposed that phosphorylation of Munc18-1 regulates neurotransmitter release (de Vries et al., 2000; Craig et al., 2003; Wierda et al., 2007; Genç et al., 2014). The initial evidence in favor of PKC involvement in PTP was that PKC inhibitors eliminate PTP, and activators (phorbol esters) occlude PTP

Received Feb. 14, 2021; revised July 3, 2021; accepted July 9, 2021.
Author contributions: C.-C.W., C.W., D.F., P.S.K., and W.G.R. designed research; C.-C.W. and C.W. performed research; C.-C.W. and C.W. analyzed data; C.-C.W., C.W., and W.G.R. wrote the paper.
D. Fioravante's present address: Center for Neuroscience, University of California, Davis, Davis, California 95618.
This work was supported by grants from the National Institutes of Health (Grants R01-NS-032405 and R35-NS-097284 to W.R.; and R01-NS-083898 to P.K.), a Goldenson Fellowship to C.C.W.; a Boehringer Ingelheim Fonds PhD Fellowship, a B&C Privatstiftung Forschungsförderung, and an Alice and Joseph Brooks Postdoctoral Fellowship to C.W.
The authors declare no competing financial interests.
Correspondence should be addressed to Wade G. Regehr at wade_regehr@hms.harvard.edu.
https://doi.org/10.1523/JNEUROSCI.0347-21.2021

(Alle et al., 2001; Rhee et al., 2002; Brager et al., 2003; Beierlein et al., 2007; Korogod et al., 2007; Lee et al., 2007; Wierda et al., 2007). Calcium-dependent PKC isoforms have been implicated in PTP at the calyx of Held (Fioravante et al., 2011) and the cerebellar parallel fiber (PF)-to-Purkinje cell (PC) synapse (Fioravante et al., 2012). The replacement of Munc18-1 with a mutated version that cannot be phosphorylated by PKC eliminated PTP at cultured hippocampal synapses (Wierda et al., 2007) and strongly attenuated PTP at the calyx of Held (Genç et al., 2014). This manipulation also eliminated or greatly reduced synaptic enhancement produced by phorbol esters (Wierda et al., 2007; Genç et al., 2014). Previous studies also implicated a number of other proteins in PTP, including calmodulin, CaMKII, myosin light chain kinase, Munc13, synaptotagmin 1, and several other candidates (Chapman et al., 1995; Rosahl et al., 1995; Wang and Maler, 1998; Junge et al., 2004; Fiumara et al., 2007; Lee et al., 2008; de Jong et al., 2016; Vandael et al., 2020).

Our goal was to test the hypothesis that PKC phosphorylation of Munc18-1 is essential to a general mechanism of PTP, and we focused on hippocampal CA3-to-CA1 synapses and cerebellar PF-to-PC synapses. Both of these synapses exhibit PTP that is thought to involve PKC (Brager et al., 2003; Fioravante et al., 2012). We could not use the approaches that had been taken to study cultured hippocampal neurons in which mutated Munc18-1 was expressed in neurons from Munc18-1 knock-out (KO) animals (Wierda et al., 2007), because Munc18-1 KO mice are embryonically lethal and individual neurons lacking Munc18-1 die (Verhage et al., 2000). In addition, CA1 pyramidal cells and cerebellar Purkinje cells receive inputs from a great many presynaptic cells, and it is difficult to express rescue constructs in a large fraction of presynaptic cells. We therefore generated a knock-in (KI) mouse (Munc18-1SA mouse) in which Munc18-1 is replaced with a mutated form that cannot be phosphorylated by PKC to study the contribution of PKC phosphorylation of Munc18-1 to PTP. We find that in Munc18-1SA mice, PTP and enhancement by phorbol esters are still largely intact for both CA3-to-CA1 and PF-to-PC synapses. This suggests that PKC phosphorylation of Munc18-1 is not the primary mechanism underlying PTP at CA3-to-CA1 and PF-to-PC synapses.

Materials and Methods

Animals. All animal experiments were completed in accordance with guidelines set by the Harvard Medical Area Standing Committee on Animals. PKC$\alpha\beta\gamma$ triple-KO (TKO) mice were obtained through the breeding of PKCα, PKCβ, and PKCγ knock-out animals (Abeliovich et al., 1993; Leitges et al., 1996; 2002). Mice of either sex were studied.

Generation of Munc18-1SA mice. Serines 306, 312, and 313, which are in exon 11 of the Munc18-1 gene, were replaced with nonphosphorylatable alanines using homologous recombination at InGenious Targeting Laboratory. Briefly, a targeting vector was constructed from a 9.53 kb fragment of a C57BL/6 BAC (bacterial artificial chromosome) clone (RP23: 320N1). The construct contained from 5′ to 3′: a 6.7-kb-long homology arm; a conditional inversion cassette with a wild-type (WT) exon 11; a neomycin resistance gene; and an inverted SA exon 11 flanked by loxp/lox2272 sites, a short homology arm, and a diphtheria toxin-expressing cassette. The targeting vector was confirmed by restriction analysis and sequencing. Hybrid (129/Sv × C57BL/6) embryonic stem (ES) cells were electroporated with the NotI-linearized targeting vector, and homologous recombined ES cell clones were identified by PCR and sequencing. Upon expansion, homologous recombination was confirmed by Southern blotting using BclI digestion of genomic DNA and a 5′ outside probe. Chimeric mice were generated by blastocyst injections and bred to C57BL/6 mice. Following confirmation of germline transmission of the mutant allele, the neomycin resistance cassette was removed by crossing the mice with flp recombinase transgenic mice (Dymecki, 1996) to generate the Munc18-1cSA allele. A heterozygous Munc18-1cSA line was maintained by crossing heterozygous Munc18-1cSA males with BL6 females. Munc18-1SA mice were generated by crossing heterozygous Munc18-1cSA males with heterozygous Munc18-1cSA/human β-actin Cre females. Sequencing (tails) and mass spectrometry (brain tissue) were used to establish that inversion of the cSA allele is efficient in Munc18-1cSA/cSA human β-actin Cre-positive mice, and these mice are referred to as Munc18-1SA mice. For individual experiments, wild-type littermate controls were used, or, if not available, age range-matched controls were used. Data analysis was pooled from all experiments.

The Munc18-1SA mice were genotyped by PCR with oligonucleotide primers (5′-TTG GAG TAG GAA TAC TGG CCC-3′ and 5′-ACA GAA GAG GAG CTG ACC CCT G-3′ to identify a 573 bp KI band and a 511 bp wild-type band. DNA sequencing (Eton Biosciences) and protein mass spectrometry analysis (Harvard Mass Spectrometry and Proteomics Resource Laboratory) confirmed that wild-type Munc18-1 had been replaced by Munc18-1-containing point mutations that eliminate PKC phosphorylation sites. Experiments were performed using Munc18-1SA mice and animals that express wild-type Munc18-1.

Measurement of motor activity. Mice between 3 and 4 weeks of age were used for motor activity assays. All behavioral experiments were conducted in the dark phase of the light/dark cycle. Individual mice were placed in a plastic chamber (23 × 16 inches) filled with standard mouse bedding. Open field activity was recorded using a USB IR-illumination camera (ELP) in near darkness for 10 min shortly after mice were placed in the chamber. The chamber was thoroughly cleaned with ethanol after each trial, and the bedding was replaced. Mouse behavior was tracked using custom scripts written in MATLAB. Analysis was conducted blind to genotype.

Preparation of brain slices. Mice of either sex aged postnatal day 12 (P12) to P15 (for cerebellar slices) or P18–P25 (for hippocampal slices) were anesthetized with isoflurane and decapitated. Acute transverse slices (hippocampal slices, 300–320 µm thick; cerebellar slices, 250 µm thick) were cut in ice-cold solution consisting of the following (in mM): 110 choline-Cl, 7 $MgSO_4$, 2.5 KCl, 1.2 NaH_2PO_4, 0.5 $CaCl_2$, 25 glucose, 11.6 Na-ascorbate, 2.4 Na-pyruvate, and 25 $NaHCO_3$. Slices were then incubated at 32°C for 20–30 min in a bicarbonate-buffered solution composed of the following (in mM): 125 NaCl, 25 $NaHCO_3$, 1.25 NaH_2PO_4, 2.5 KCl, 1.5 $CaCl_2$ (2 $CaCl_2$ for cerebellar slices), 1.5 $MgCl_2$ (1 $MgCl_2$ for cerebellar slices), and 25 glucose. The slices were kept in the chamber at room temperature until recording or protein extraction.

Electrophysiology. The recordings for hippocampal CA3-to-CA1 synapses were performed as described previously (Wang et al., 2016). Briefly, recordings were conducted at 30–32°C, and the hippocampal CA3 region was cut from the CA1 region with a scalpel blade to prevent recurrent excitation. The external solution was the same solution used for incubating slices but was supplemented with the following drugs (in µM): 20 bicuculline, 2 CGP, 2 CPP, and 1 AM251. A stimulation electrode filled with ACSF was placed at least 500 µm away from the recording site to stimulate the Schaffer collateral fibers. For field recordings, the recording pipettes (0.3–2 MΩ) were filled with ACSF and placed in the stratum radiatum in the CA1 dendritic area, and an input–output curve with a stimulation range of 10–80 µA was first analyzed to determine the stimulation intensity that produced approximately half of the maximum response without evoking population spikes. Recordings of granule cell parallel fiber-to-PC synapses were made as described previously (Fioravante et al., 2012). The internal solution consisted of 100 (in mM) CsCl, 35 CsFl, 10 EGTA, 10 HEPES, and 3 or 5 QX-314-Cl (Fioravante et al., 2012; Weyrer et al., 2019). PF-to-PC experiments were performed at 30–36°C. Miniature EPSCs (mEPSCs) were recorded in whole-cell configuration using 2 MΩ pipettes filled with the same internal solution used to measure evoked EPSCs. TTX (1 µM) was added to the external solution to block action potential-evoked synaptic currents. Data were recorded in 30 s epochs, sampled at 2.5 kHz, and filtered at 500 Hz with an eight-pole Bessel filter (Frequency Devices). Membrane potential was maintained at −70 mV.

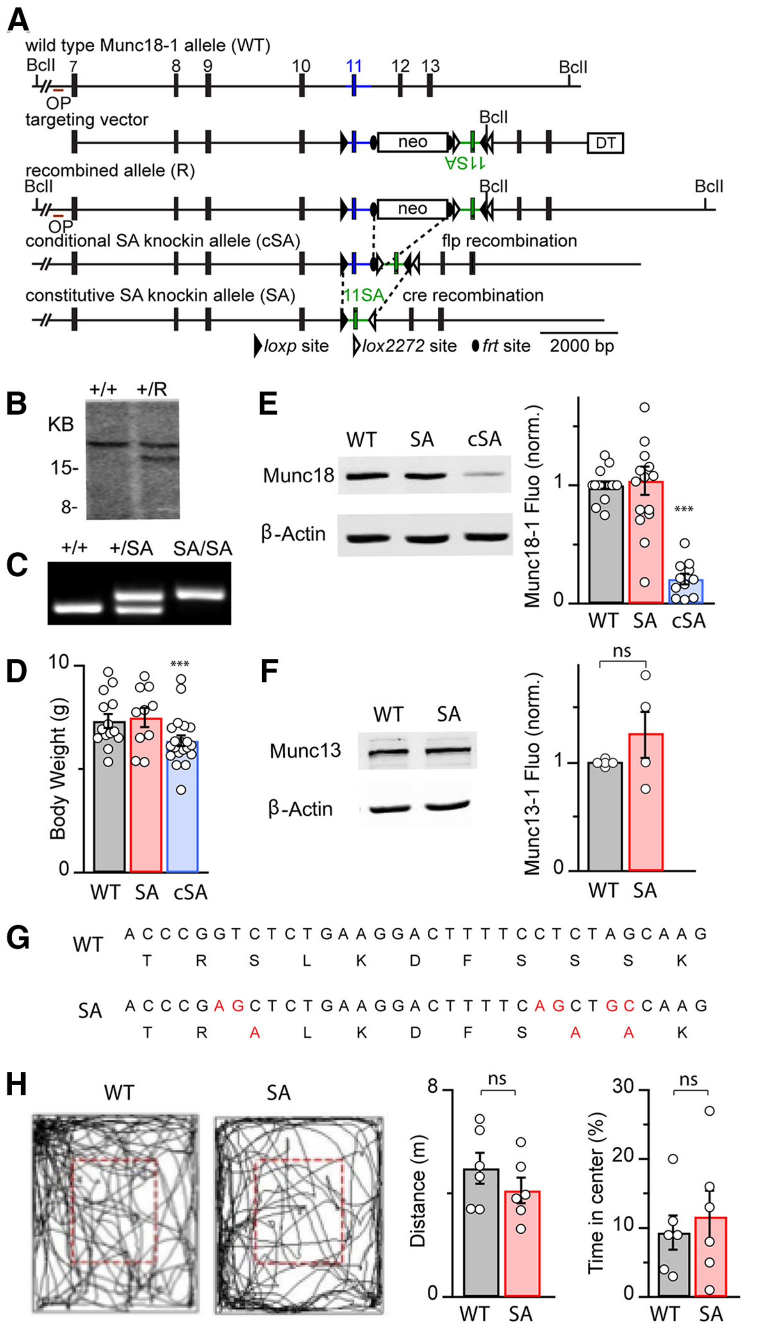

Figure 1. Generation and basic characterization of Munc18-1SA mice. ***A***, Knock-in strategy for Munc18-1SA mice. DT, Diptheriatoxin-expressing cassette; neo, neomycin resistance cassette. ***B***, Southern blot of DNA digested with BclII from embryonic stem cells from wild-type controls and heterozygous cells after homologous recombination. ***C***, PCR genotyping of wild-type mice, heterozygous Munc18-1SA mice, and homozygous Munc18-1SA mice. ***D***, Body weights of (P12–P15) wild-type, Munc18-1SA, and Munc18-1cSA mice. ***E***, Left, Western blots of brain homogenates for wild-type, Munc18-1SA, and Munc18-1cSA mice. Right, Summary of Munc18-1 expression levels assessed by Western blotting with fluorescent secondary antibodies. ***F***, Left, Western blots of brain homogenates for wild-type and Munc18-1SA mice. Right, Summary of Munc13-1 expression levels assessed by Western blotting with fluorescent secondary antibodies. ***G***, DNA (top) and protein (bottom) sequencing are shown for wild-type and Munc18-1SA mice, with altered regions highlighted (red). ***H***, Left, Open field assay examples for a wild-type and a Munc18-1SA mouse. Right, Summaries of the total distance traveled in 10 min and the percentage of time spent in the center (within the red dashed line).

Series resistance compensation was not used. Leak currents were −10 to −200 pA. Events were counted and analyzed offline using IGOR PRO software (WaveMetrics, Harvard Medical School, Boston MA) and custom macros provided by Monica Thanawala. Inclusion criteria were a 4–10 pA amplitude threshold, a minimum rate of rise of 0.4 pA/ms, and a decay time constant between 3 and 12 ms. At least two trials were recorded for each cell to obtain the average mEPSC frequency and amplitude.

For cerebellar experiments, stimuli were given every 2.5 s, then 10 PTP-inducing stimuli at 50 Hz were applied 2.5 s after the last EPSC of the baseline. One second after the train, stimuli were resumed and delivered every 2.5 s. The stimulus intensity was adjusted to have the initial stimulus evoke an EPSC of ∼150–400 pA.

Recordings (see Fig. 5*A*,*B*) were performed blind to genotype. Other datasets consist of blinded and unblinded experiments and are therefore considered unblinded to genotype. Data are expressed as the mean ± SEM.

Western blotting. Western blotting was conducted as described previously (Wang et al., 2016). Brains, excluding cerebellum, were extracted acutely from animals that were 2–3 weeks of age and homologized in ice-cold lysis buffer containing 150 mM NaCl, 25 mM HEPES, 4 mM EGTA, phosphatase inhibitor (catalog #04906845001, Roche), and protease inhibitor (catalog #P8340, Sigma-Aldrich). Total protein concentration was determined by a BCA Assay (Thermo Fisher Scientific), and 30 μg of protein in Laemmli sample buffer was loaded onto 10% polyacrylamide gels (Bio-Rad). After SDS-PAGE, gels were transferred onto nitrocellulose membranes and blocked in 5% nonfat milk (Cell Signaling Technology) in TBS-Tween 20 (TBST). Membranes were incubated overnight at 4°C with primary antibodies, followed by incubation with fluorescent secondary antibodies for 1.5 h. Membranes were washed with TBST several times followed by 2× washing in TBS. Membranes were dried and imaged in Odyssey Classic imaging system (LI-COR). Nonsaturated images were quantified in ImageJ. Analysis was conducted blind to genotype. For analysis, the fluorescent intensities of target bands were measured blind to genotype and then normalized to β-actin fluorescence intensity. These values were further normalized to the averaged wild-type control values in the same gel. Data are expressed as the mean ± SEM, and statistical analyses were conducted using a one-way ANOVA (Fig. 1*E*) and paired *t* tests (Fig. 1*F*). The following antibodies were used: Munc18-1 (1:1000; catalog #ab3451, Abcam); β-actin (1:5000; Sigma, catalog #A1978); Munc13-1 (1:1000 Synaptic Systems, catalog #126102); rabbit phospho- and fluorescent antibodies (1:10,000; IRDye 800CW Donkey anti-Rabbit IgG; catalog #926–32213, LI-COR; and IRDye 680RD Donkey anti-Mouse IgG; catalog #926–68072, LI-COR).

Mass spectrometry. A total of 2.5 μl of Munc18-1 antibody was added to 500 μg of brain lysate, followed by the incubation at 4°C for overnight. Protein lysate was extracted in ice-cold lysis buffer containing 150 mm NaCl, 25 mm HEPES, 4 mm EGTA, phosphatase inhibitor (catalog #04906845001, Roche), and protease inhibitor (catalog #P8340, Sigma-Aldrich). Total protein concentration was determined by a BCA assay (Thermo Fisher Scientific), and 60 μl Protein A beads with 50% slurry (catalog #9863S, Cell Signaling Technology) were then added and incubated for 6 h to pull down the antibody–protein complex. Beads were then washed with PBS and subjected to SDS-PAGE. The gel was stained with Coomassie Blue, and the band that corresponds to Munc18-1 molecular weight was cut. That band was subjected to mass spectrometry analysis by the Harvard Mass Spectrometry and Proteomics Resource Laboratory.

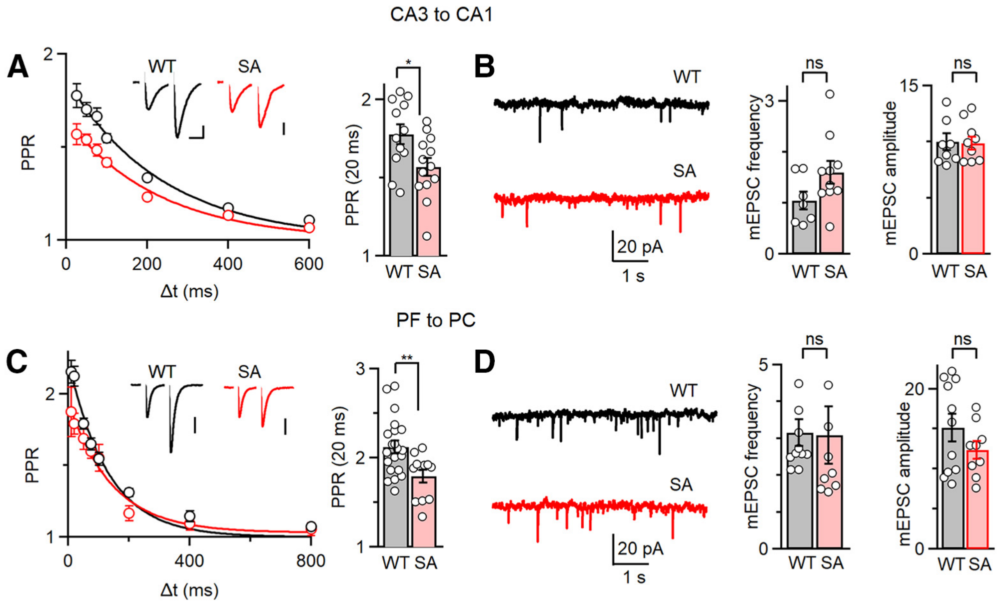

Figure 2. Basal synaptic properties in Munc18-1 SA-KI mice. ***A***, Paired-pulse facilitation in wild-type and Munc18-1 SA KI mice at CA3-to-CA1 synapses. Insets show representative synaptic currents evoked by pairs of stimuli separated by 20 ms. The decay of PPR was fit with a single exponential with a time constant of 240 ms for WT and 230 ms for Munc18-1SA mice. Calibration: 100 pA. Horizontal scale bars: ***A***, inset (for ***A***, ***C*** insets), 10 ms. ***B***, Example spontaneous mEPSCs in wild-type and Munc18-1SA mice (left) and summaries of mEPSC frequencies and amplitudes (right). ***C***, ***D***, Same as ***A*** and ***B*** except for the cerebellar granule cell-to-Purkinje cell synapse. The decay of PPR was fit with a single exponential with a time constant of 129 ms for WT and 143 ms for Munc18-1SA mice. See Table 1.

Results

Generation and initial characterization of Munc18-1SA mice

To study the role of PKC phosphorylation of Munc18-1, we used homologous recombination to generate conditional knock-in mice in which Munc18-1 cannot be phosphorylated by PKC. This was achieved by using homologous recombination in embryonic stem cells to replace serines 306, 312, and 313 that can be phosphorylated by PKC (de Vries et al., 2000; Craig et al., 2003; Wierda et al., 2007) with nonphosphorylatable alanines (Munc18-1SA: S306A/S312A/S313A; Fig. 1*A*). Successful recombination was confirmed first by PCR and DNA sequencing, and by Southern blotting (Fig. 1*B*). Chimeric mice with the Munc18-1 recombined (R) allele were obtained by blastocyst injection. Upon germline transmission, the neomycin-resistance cassette was removed by flp recombination using transgenic mice (Dymecki, 1996) to produce the conditional SA knock-in allele (cSA; Fig. 1*C*). Munc18-1cSA mice had an 18% reduced body weight ($n = 21$, $p < 0.001$; Fig. 1*D*), and were hypomorphic, expressing only 23% of Munc18-1 in control mice ($n = 11$, $p < 0.001$; Fig. 1*E*). Cre-recombination was performed using transgenic mice (Lewandoski and Martin, 1997) to generate Munc18-1SA mice (SA), which recovered Munc18-1 expression levels and body weight to control levels, and the offspring of heterozygote matings survived at Mendelian ratios (of 258 mice, 61 were WT, 69 were SA, and 128 were heterozygotes). Levels of the key presynaptic protein Munc13-1 were not significantly different in Munc18-1SA animals ($n = 4$, $p = 0.23$; Fig. 1*F*). Sequencing of the Munc18-1 PCR product and mass spectrometry of brain protein extracts confirmed that serines 306, 312, and 313 were replaced by alanines in these mice (Fig. 1*G*).

There were no obvious behavioral deficits. Motor activity was assessed in open field tests and was similar in littermate controls and Munc18-1SA mice (Fig. 1*H*). The distance traveled in 10 min was 4.98 ± 0.60 m ($n = 6$) for littermate controls and 4.13 ± 0.49 m ($n = 6$) for Munc18-1SA mice ($p = 0.3$). Both genotypes spent similar amounts of time in the center (WT: 9.3 ± 2.5%, $n = 6$; Munc18-1SA: 11.7 ± 3.8%, $n = 6$; $p = 0.6$).

These findings indicate that Munc18-1SA mice are global knock-in mice in which wild-type Munc18-1 has been replaced by Munc18-1SA, and the expression levels of Munc18-1 are unchanged. These mice are therefore well suited to our primary goal, which was to determine the effect of Munc18-1 phosphorylation on synaptic transmission. The observation that in the absence of Cre the Munc18-1cSA mice are hypomorphs indicates that this mouse is not suitable for our secondary goal, which was to have a mouse that would allow us to selectively replace Munc18-1 with Munc18-1SA in a Cre-dependent manner while leaving WT Munc18-1 at normal levels in other cells.

Basal properties of synaptic transmission

Before examining PTP, we characterized basal synaptic properties. We began by characterizing paired-pulse plasticity. At both CA3-to-CA1 synapses and PF-to-PC synapses, the second of two closely spaced stimuli evoked a larger response than the first as a result of facilitation. Changes in the paired-pulse ratio (PPR) could arise either directly, by contributing to facilitation, or indirectly, by altering the initial probability of release (Zucker and Regehr, 2002). PKC phosphorylation of Munc18-1 has not been implicated in facilitation, which is thought to be mediated by synaptotagmin 7 at the CA3-to-CA1 synapse (Jackman et al., 2016). Alternatively, the most common means of altering PPR is by changing the initial probability of release (p): an increase in the initial p value indirectly decreases PPR and vice versa, in part because vesicle depletion is more prominent when the initial p value is high (Zucker and Regehr, 2002). We stimulated synaptic inputs with pairs of pulses separated by 20–600 ms. At the CA3-to-CA1 synapse, for stimuli separated by 20 ms the PPR was 1.78 ± 0.06 in littermate controls (N = 4 animals, $n = 12$ cells) and was moderately but statistically significantly reduced in Munc18-1SA mice (1.57 ± 0.06, $N = 4$, $n = 13$; Fig. 2*A*, Table 1). At the PF-to-PC synapse, the magnitude of facilitation was

Table 1. Data summary for Figure 2

Synapses		WT	Munc18-1SA	p Value
CA3 to CA1	mEPSC frequency	1.05 ± 0.18 (n = 7)	1.60 ± 0.22 (n = 10)	0.07
	mEPSC amplitude	10.00 ± 0.77 pA (n = 7)	9.99 ± 0.56 pA (n = 10)	0.90
	PPR (20 ms interval)	1.78 ± 0.06 (n = 12)	1.57 ± 0.06 (n = 13)	0.02
PF to PC	mEPSC frequency	3.16 ± 0.36 (n = 11)	3.10 ± 0.78 pA (n = 9)	0.90
	mEPSC amplitude	15.2 ± 3.2 pA (n = 11)	12.4 ± 3.1 pA (n = 9)	0.19
	PPR (20 ms interval)	2.12 ± 0.07 (n = 21)	1.79 ± 0.07 (n = 12)	0.004

also statistically significantly reduced from 2.12 ± 0.07 (N = 7, n = 21) in littermate controls to 1.79 ± 0.07 (N = 4, n = 12) in Munc18-1SA mice (Fig. 2*C*, Table 1). These findings are consistent with a slight increase in the basal probability of release or with with direct effects on paired-pulse plasticity at these synapses in Munc18-1SA mice.

We also tested the possibility that the initial probability of release was altered in Munc18-1SA mice by determining the input–output curve at the CA3-to-CA1 synapse. We stimulated CA3 axons with a range of intensities and recorded the resulting responses. The presynaptic volley provides a measure of the number of activated fibers, and the field EPSP (fEPSP) provides a measure of synaptic strength (Dingledine and Somjen, 1981). If the initial probability of release were increased, then this ratio would also be increased. We found that the ratio of the amplitude of the fEPSP versus the amplitude of the presynaptic volley was 1.88 ± 0.29 (n = 14) for WT mice and 2.46 ± 0.20 (n = 14) for Munc18-1SA mice, but they were not significantly different (p = 0.38, Wilcoxon rank-sum test). Thus, despite a trend toward an increase in the ratio of the amplitude of the fEPSP/the amplitude of the presynaptic volley, it is not significantly increased.

We also examined the spontaneous neurotransmitter release of mEPSCs in the presence of TTX. There was no statistically significant difference in either the amplitudes or the frequencies of mEPSCs for littermate controls and Munc18-1SA mice for CA3-to-CA1 synapses (Fig. 2*B*) and PF-to-PC synapses (Fig. 2*D*). Thus, the basal properties of spontaneous neurotransmitter release are not altered at these synapses in Munc18-1SA mice (Table 1).

Phorbol ester-mediated enhancement

PKC can be activated by either calcium ions or the second messenger diacylglycerol (DAG) produced by phospholipase C (Zeng et al., 2012). The phorbol ester PDBu mimics DAG and activates PKC by binding to the C1 domain of PKC. It has been proposed that PDBu enhances transmission by activating PKC and phosphorylating Munc18-1 in much the same way that elevations of presynaptic calcium can enhance the transmission in PTP. At many synapses, phorbol esters both enhance transmission and occlude PTP (Malenka et al., 1986; Shapira et al., 1987; Saitoh et al., 2001; Lou et al., 2005; Korogod et al., 2007). This implicates PKC in both forms of enhancement, but the interpretation of such occlusion experiments is complicated because PDBu can also activate proteins other than PKC that contain a C1 domain, such as Munc13 (Hori et al., 1999; Brose and Rosenmund, 2002; Rhee et al., 2002; Junge et al., 2004; Wierda et al., 2007; Lou et al., 2008; Broeke et al., 2010; de Jong et al., 2016).

Previous studies concluded that phorbol ester-mediated enhancement of mEPSC frequency was entirely dependent on PKC phosphorylation of Munc18-1 for cultured hippocampal cells (Wierda et al., 2007), but at the calyx of Held only half of the enhancement was mediated by this mechanism (Genç et al., 2014). These studies either expressed a PKC-insensitive Munc18-1 in a null background for cultured hippocampal cells or conditionally eliminated Munc18-1 and virally expressed a PKC-insensitive Munc18-1 at the calyx of Held. Here we use Munc18-1SA mice to perform similar experiments at CA3-to-CA1 synapses and PF-to-PC synapses. We found that at the CA3-to-CA1 synapse PDBu produced large increases in the mEPSC frequency in both control mice (9.04 ± 0.83-fold increase, N = 2, n = 10) and Munc18-1SA mice (12.82 ± 0.75-fold increase, N = 2, n = 10; Fig. 3*A*, Table 2). There was no statistically significant difference in the magnitude of enhancement in littermate controls and Munc18-1SA-KI mice (p = 0.30). We found that PDBu also increased mEPSC frequency at the PF-to-PC synapse in both littermate controls (2.53 ± 0.56-fold) and Munc18-1SA mice (3.88 ± 0.26, N = 2, n = 7; Fig. 3*C*). This indicates that PKC phosphorylation of Munc18-1 does not account for the enhancement of mEPSC frequency by phorbol esters at the PF-to-PC synapse.

At the CA3-to-CA1 synapse, there was no statistically significant difference in the extent of PDBu enhancement of fEPSPs in control mice (2.42 ± 0.52, N = 5, n = 12) and Munc18-1SA mice (1.64 ± 0.33 N = 4, n = 10, p = 0.23; Fig. 3*B*). PDBu also decreased the PPR to a similar extent in control and Munc18-1SA mice (Fig. 3*B*). At the PF-to-PC synapse, PDBu enhanced transmission by 3.07 ± 0.32-fold (N = 6, n = 13) in wild-type animals and by 2.87 ± 0.33-fold (N = 3, n = 7) in Munc18-1SA mice (Fig. 3*D*). Our findings indicate that PKC phosphorylation of Munc18-1 plays either a modest role or no role in PDBu-dependent enhancement of spontaneous and evoked synaptic transmission at CA3-to-CA1 and PF-to-PC synapses.

PTP

We examined the role of Munc18-1 phosphorylation in PTP at the CA3-to-CA1 synapse. A pharmacological study previously implicated PKC in PTP at this synapse (Brager et al., 2003), but we recently found that PTP is not dependent on calcium-dependent PKC isoforms (Wang et al., 2016). We found that 50 stimuli at 50 Hz produced synaptic enhancement (fEPSC amplitudes increased by 67 ± 9%, N = 4, n = 11) that decayed with a time constant of 9.9 ± 0.7 s (Fig. 4*A*,*C*, Table 3). PTP was accompanied by a decrease in PPR such that the PPR 5 s after tetanic stimulation divided by the PPR before tetanic stimulation was 0.79 ± 0.02, and it recovered with a time constant (τ) of 11.1 s. This decrease in PPR is consistent with a transient elevation in release probability that has been shown to accompany PTP at some synapses (Zucker and Regehr, 2002). The amplitude of PTP was significantly different in Munc18-1SA animals (46 ± 5% enhancement, N = 5, n = 16, p = 0.04), and PTP was significantly shorter lived (τ =7.6 ± 0.5 s, p = 0.0095), and was also accompanied by a decrease in PPR (0.80 ± 0.01, τ = 9.1 s; Fig. 4*B*,*C*). These results indicate that although there is a significant decrease in the amplitude and time course of PTP, most PTP at the CA3-to-CA1 synapse is not reliant on PKC phosphorylation of Munc18-1.

We also assessed the occlusion of PTP by phorbol esters at CA3-to-CA1 synapses. The observation that phorbol esters occlude PTP could arise either from PKC activation and Munc18-1 phosphorylation (Wierda et al., 2007; Genç et al., 2014) or from an alternative mechanism such as PKC phosphorylation of another protein or phorbol ester activation of another protein (Brose and Rosenmund, 2002; Rhee et al., 2002; de Jong and Fioravante, 2014; de Jong et al., 2016). To determine whether PDBu occludes PTP by phosphorylating

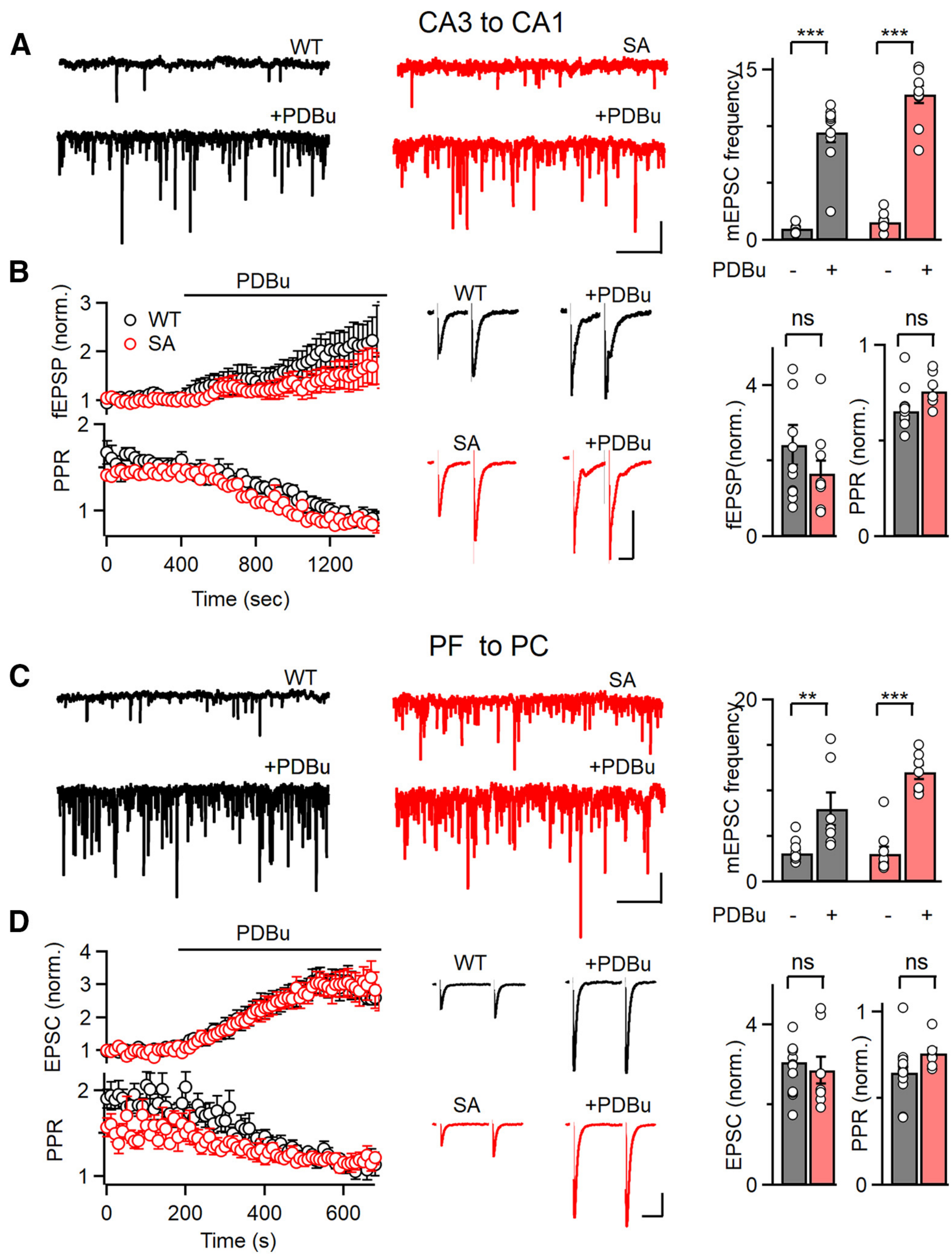

Figure 3. Phorbol esters enhance synaptic transmission in Munc18-1SA mice. ***A***, The effect of the phorbol ester PDBu on mEPSCs recorded in CA1 pyramidal cells in the presence of TTX are shown for representative experiments before and during PDBu application (left and middle), and bar graphs summarize the results (right). ***B***, The effects of phorbol ester PDBu on fEPSP amplitudes and paired pulse plasticity at CA3-to-CA1 synapses for wild-type and Munc18-1SA mice. Summaries showing wash-ins (left), traces from representative experiments (middle), and bar graph summaries (right) are shown. ***C***, ***D***, Same as ***A*** and ***B*** but for Purkinje cells and the granule cell-to-PC synapse. In ***D***, EPSCs were measured in voltage clamp. See Table 2.

Munc18-1, we compared the occlusion in littermate controls and Munc18-1SA mice (Fig. 4*D–F*). PTP was much smaller in the presence of PDBu for both wild-type mice (PDBu: 1.14 ± 0.03, $n = 9$, $N = 4$; vehicle: 1.67 ± 0.09, $n = 11$, $N = 4$) and Munc18-1SA mice (PDBu: 1.08 ± 0.03, $n = 10$, $N = 4$; vehicle: 1.46 ± 0.05, $n = 16$, $N = 5$). These findings indicate that PDBu occlusion of PTP at this synapse is not a result of phorbol esters activating PKC to phosphorylate Munc18-1.

We went on to examine PTP at the PF-to-PC synapse, where PKC has also been implicated in PTP. PTP was induced by a rather short stimulus train (10 stimuli at 50 Hz) to avoid producing presynaptic LTP (Fig. 5*A*, Table 4). PTP was still present in Munc18-1SA animals with peak levels of PTP slightly larger than in wild-type animals (Fig. 5*B*,*D*). Thus, preventing PKC phosphorylation of Munc18-1 does not reduce PTP at the PF-to-PC synapse.

PTP at PF-to-PC synapses can also be mediated by a compensatory mechanism that is independent of PKC (Fioravante et al., 2012). This is illustrated by comparing the effect of the broad-spectrum PKC inhibitor GF109203X (GF) on PTP in wild-type animals and animals without calcium-dependent PKC isoforms. GF eliminates PTP in wild-type animals, which suggests that PKC is required for PTP at this synapse in wild-type animals. When calcium-dependent PKC isoforms are removed in PKCα,

Table 2. Data summary for Figure 3 Summary of the effects of phorbol esters on spontaneous and evoked transmission at CA3-to-CA1 synapses and PF-to-PC synapses

	Control			Munc18-1SA			
	Control	PDBU	Normalized (PDBU/control)	Control	PDBu	Normalized (PDBU/control)	p Value (WT vs KI)
mEPSC frequency							
CA3 → CA1	1.05 ± 0.18 (n = 7; N = 2)	9.48 ± 0.87 (n = 10; N = 2)	9.04 ± 0.83 (n = 10; N = 2) p < 0.001	1.60 ± 0.22 (n = 10; N = 2)	12.82 ± 0.75 (n = 10; N = 2)	8.01 ± 0.47 (n = 10; N = 2) p < 0.001	p = 0.3
PF → PC	3.16 ± 0.36 (n = 11; N = 2)	7.98 ± 1.78 (n = 7; N = 2)	2.53 ± 0.56 (n = 7; N = 2) p < 0.03	3.10 ± 0.78 (n = 9; N = 2)	12.02 ± 0.80 (n = 7; N = 2)	3.88 ± 0.26 (n = 7; N = 2) p < 0.001	p = 0.05
Evoked response							
CA3 → CA1			2.42 ± 0.51 (n = 12; N = 5) p < 0.01			1.64 ± 0.34 (n = 8; N = 4) p < 0.01	p = 0.23
PF → PC			3.07 ± 0.32 (n = 13; N = 5) p < 0.001			2.87 ± 0.33 (n = 8; N = 3) p < 0.001	p = 0.68
PPR							
CA3 → CA1	1.68 ± 0.13 (n = 12; N = 5)	0.94 ± 0.03 (n = 12; N = 5)	0.62 ± 0.03 (n = 12; N = 5) p < 0.001	1.41 ± 0.04 (n = 8; N = 4)	0.79 ± 0.05 (n = 8; N = 4)	0.57 ± 0.03 (n = 8; N = 4) p < 0.001	p = 0.23
PF → PC	1.83 ± 0.08 (n = 13; N = 5)	1.20 ± 0.07 (n = 13; N = 5)	0.65 ± 0.03 (n = 13; N = 5) p < 0.001	1.55 ± 0.08 (n = 8; N = 3)	1.17 ± 0.04 (n = 8; N = 3)	0.76 ± 0.03 (n = 8; N = 3) p < 0.001	p = 0.03

p Values were obtained using two-way ANOVA and Tukey's multiple-comparisons test.

PKCβ, and PKCγ TKO animals (PKC$\alpha\beta\gamma$ TKO animals), PTP is still present at the PF-to-PC synapse, but it is insensitive to GF (Fig. 5*C*,*D*), which is similar to PKC$\alpha\beta$ double-KO (DKO) animals (Fioravante et al., 2012). These findings suggest that PTP is mediated by a PKC-dependent mechanism in wild-type animals, and by a compensatory PKC-independent mechanism in PKC$\alpha\beta\gamma$ TKO animals, (as in PKC$\alpha\beta$ DKO mice; Fioravante et al., 2012). It is not clear whether the PTP present in Munc18-1SA animals is mediated by PKC phosphorylation of a target other than Munc18-1 or is mediated by a PKC-independent compensatory mechanism, as in the PKC$\alpha\beta\gamma$ TKO animals. GF can be used to distinguish between these possibilities: if PTP in Munc18-1SA animals is blocked by GF, it is consistent with the former possibility, whereas if PTP in Munc18-1SA animals is insensitive to GF, it is consistent with the latter possibility.

We confirmed that GF strongly attenuates PTP in WT mice and found that it also strongly attenuated PTP in Munc18-1SA animals (Fig. 5*C*). These experiments also revealed that the first EPSC recorded after tetanic stimulation was still enhanced in both wild-type and SA mice in the presence of GF. For that reason, we compared the second EPSC (t = 4.1 s), which provides a better measure of the longer-lasting enhancement typical of augmentation and PTP (Fig. 5*D*). This suggests that at PF-to-PC synapses in Munc18-1SA animals almost all of the PTP relies on PKC. A comparison of PTP in WT and Munc18-1SA animals in control conditions and in the presence of GF illustrates the differences in amplitudes and time courses of PTP. These results indicate that at PF-to-PC synapses, PTP is not reliant on PKC phosphorylation of Munc18-1 and suggest that PKC produces PTP at this synapse by phosphorylating a different target.

Discussion

We assessed a mechanism of PTP in which calcium enters the presynaptic terminal and activates calcium-dependent PKC, which in turn phosphorylates Munc18-1 to enhance synaptic transmission. Our findings indicate that at CA3-to-CA1 and PF-to-PC synapses, phorbol ester-dependent enhancement and PTP are mediated primarily by mechanisms that do not involve PKC phosphorylation of Munc18-1.

PKC phosphorylation of Munc18-1 and basal transmission

Our findings indicate that any effects on basal transmission at CA3-to-CA1 and PF-to-PC synapses in Munc18-1SA mice are small. The lack of alterations in spontaneous release rates and in mEPSC sizes suggests that the total number of release sites onto a cell that give rise to mEPSCs is not altered, and that there are no postsynaptic changes in Munc18-1SA mice. The small decrease in paired-pulse plasticity in Munc18-1SA mice could reflect either an increase in the basal probability of release or a direct effect on paired-pulse plasticity. Our attempt at distinguishing between these possibilities by measuring the fEPSP amplitude/presynaptic volley ratio was inconclusive. This ratio is expected to increase if the initial probability of release is elevated, but we found that there was an increase in the fEPSP amplitude/presynaptic volley ratio that was not statistically significant. Although the precise manner in which paired-pulse plasticity is altered in Munc18-1SA mice remains uncertain, it is clear that any effect of Munc18-1 phosphorylation on basal synaptic transmission is small.

PKC phosphorylation of Munc18-1 and PTP

Our results establish that most PTP at the CA3-to-CA1 synapse is not reliant on PKC phosphorylation of Munc18-1. PKC was initially implicated in PTP at the CA3-to-CA1 synapse by a pharmacological study showing that phorbol esters enhance transmission and occlude PTP, and that PKC inhibitors block PTP (Brager et al., 2003). A subsequent study confirmed these findings in wild-type animals, but found similar results in PKC$\alpha\beta\gamma$ TKO mice that lack calcium-dependent PKC isoforms (Wang et al., 2016). This indicates that calcium-dependent PKC isoforms are not the calcium sensors for PTP at this synapse and left open the following two possibilities: (1) calcium-insensitive PKC isoforms mediate PTP; or (2) PKCs are not involved in PTP at this synapse, and phorbol esters and PKC inhibitors act on proteins other than PKC. The most straightforward interpretation of the reduction of PTP in Munc18-1SA animals is that a small component of PTP relies on nonclassical PKCs phosphorylating Munc18-1. It is also possible that in Munc18-1SA animals PTP could require nonclassical PKCs phosphorylating targets other than Munc18-1 or could be mediated by a PKC-independent mechanism.

PTP at PF-to-PC synapses is also mediated primarily by mechanisms that do not rely on PKC phosphorylation of Munc18-1, but the role of PKC and Munc18-1 differs from that present at the CA3-to-CA1 synapse. At PF-to-PC synapses, when calcium-dependent PKCs are eliminated, PTP is still

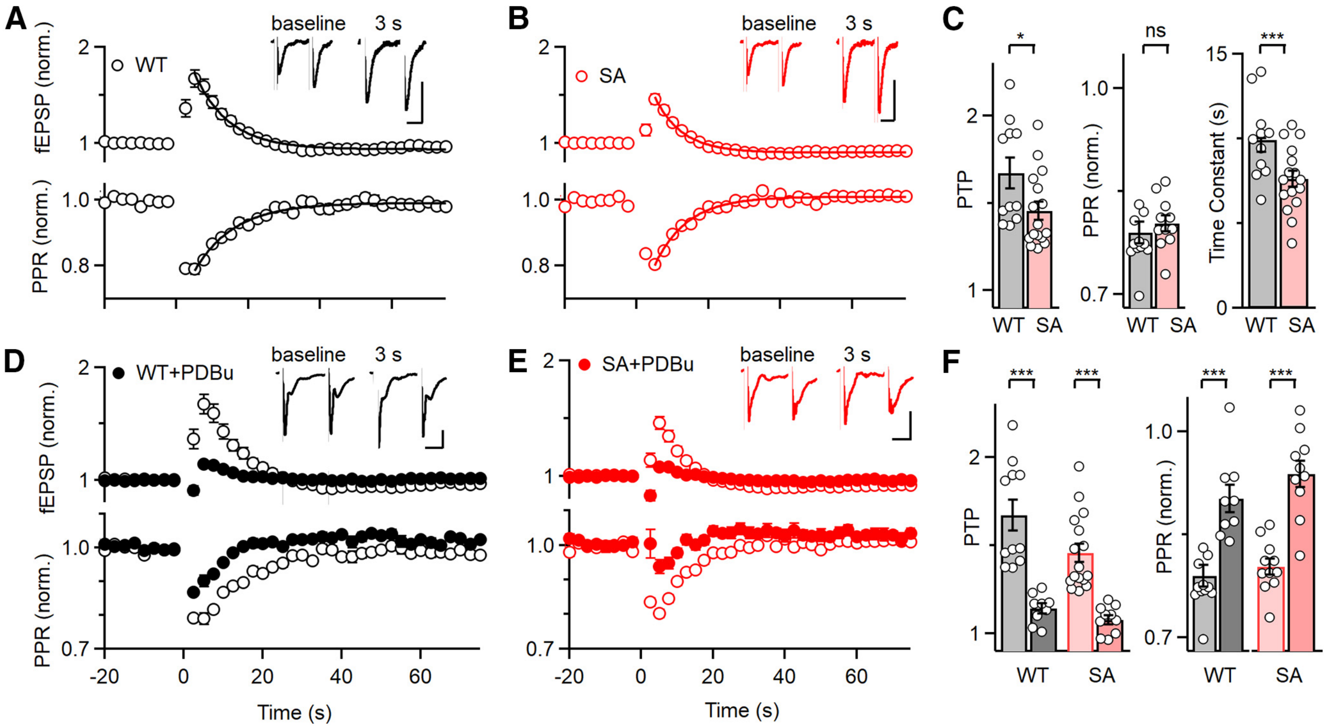

Figure 4. PTP is present at CA3-to-CA1 synapses in Munc18-1SA mice. ***A***, PTP evoked by 50 stimuli at 50 Hz in WT mice with fEPSP amplitudes and paired-pulse plasticity summarized. Inset, Responses to pairs of stimuli before tetanic stimulation (gray traces) and 3 s after (black traces). Calibration: 0.2 mV, 20 ms. ***B***, Same as in ***A*** but for Munc18-1SA mice (red), with the WT data replotted (black). The decays of PTP and changes in PPR were approximated with exponential fits (see text). ***C***, Summary of individual experiments for ***A*** and ***B***. ***D***, PTP in wild-type mice measured in control conditions (open symbols) and in the presence of PDBu (solid symbols). ***E***, As in ***D*** but for Munc18-1SA mice. ***F***, Summary of individual experiments for ***D*** and ***E***. See Table 3.

Table 3. Data summary for Figure 4 Magnitude of PTP at CA3-to-CA1 synapses data summary

	WT	SA	WT vs SA	WT, PPR	SA, PPR	WT vs SA	WT τ (s)	SA τ (s)	WT vs SA
Control	1.67 ± 0.09 ($n = 11$; $N = 4$)	1.46 ± 0.05 ($n = 16$; $N = 5$)	$p = 0.04$	0.78 ± 0.01	0.80 ± 0.01	$p = 0.59$	9.9 ± 0.7	7.6 ± 0.5	$p = 0.0095$
PDBu	1.14 ± 0.03 ($n = 9$; $N = 4$)	1.08 ± 0.03 ($n = 10$; $N = 4$)	$p = 0.90$	0.90 ± 0.02	0.94 ± 0.02	$p = 0.39$			
Control vs PDBu	$p < 0.001$	$p < 0.001$		$p < 0.001$	$p < 0.001$				

p Values were obtained using two-way ANOVA and Tukey's multiple-comparisons test.

present. The PKC inhibitor GF blocks PTP when calcium-dependent PKCs are present, but not when they are absent (Fioravante et al., 2012; Fig. 5*C*). This suggests that PKC is essential for PTP in wild-type animals, but a compensatory PKC-independent mechanism mediates PTP in PKC$\alpha\beta\gamma$ TKO mice. The compensatory mechanism that mediates PTP in the absence of calcium-dependent PKCs is not known, and there are many candidates, including the hundreds of phosphorylation sites on presynaptic proteins that are upregulated or downregulated in a calcium-dependent manner (Kohansal-Nodehi et al., 2016). In Munc18-1SA mice, PTP is intact at the PF-to-PC synapse, and no such compensation is apparent. The PTP that remains is mostly blocked by GF, suggesting that it is mediated primarily by a PKC-dependent mechanism. It appears that most PTP is mediated by PKC, but presumably as a result of phosphorylation of a protein other than Munc18-1. There are many candidates known to be phosphorylated by PKC, including SNAP25 (Shimazaki et al., 1996), synaptobrevin (Nielander et al., 1995), Liprin-a3 (Kohansal-Nodehi et al., 2016; Emperador-Melero et al., 2021), and synaptotagmin 1 (de Jong et al., 2016) . Further studies are required to determine whether PKC phosphorylation of any of these targets contributes to PTP.

The modest contribution of PKC phosphorylation of Munc18-1 to PTP we describe here for CA3-to-CA1 and PF-to-PC synapses contrasts with previous studies at cultured hippocampal synapses (Wierda et al., 2007) and at the calyx of Held in brain slices (Genç et al., 2014). In hippocampal cultures, PTP induced by 20 or 200 stimuli at 40 Hz was present at WT synapses but was completely eliminated at Munc18-1SA (referred to as M18-1_{PKCi}) synapses. At the calyx of Held, Munc18-1 was eliminated in conditional KO mice by expressing Cre in presynaptic cells and by using viruses to express either WT Munc18-1 or Munc18-1SA. WT rescue was enhanced by 120% compared with 50% for the SA rescue, and PTP decayed much more rapidly for the SA rescue such that the 60% reduction in initial PTP amplitude corresponded to an 84% reduction in the cumulative PTP. It was therefore concluded that PTP at the calyx of Held was a consequence of PKC phosphorylation of Munc18-1, with phosphorylation and enhancement persisting until phosphatases dephosphorylated Munc18-1. These results suggested that PKC phosphorylation of Munc18-1 accounted for all of the PTP for cultured hippocampal synapses and most of the PTP at the calyx of Held. Our results combined with these previous results indicate that PKC phosphorylation of Munc18-1 makes

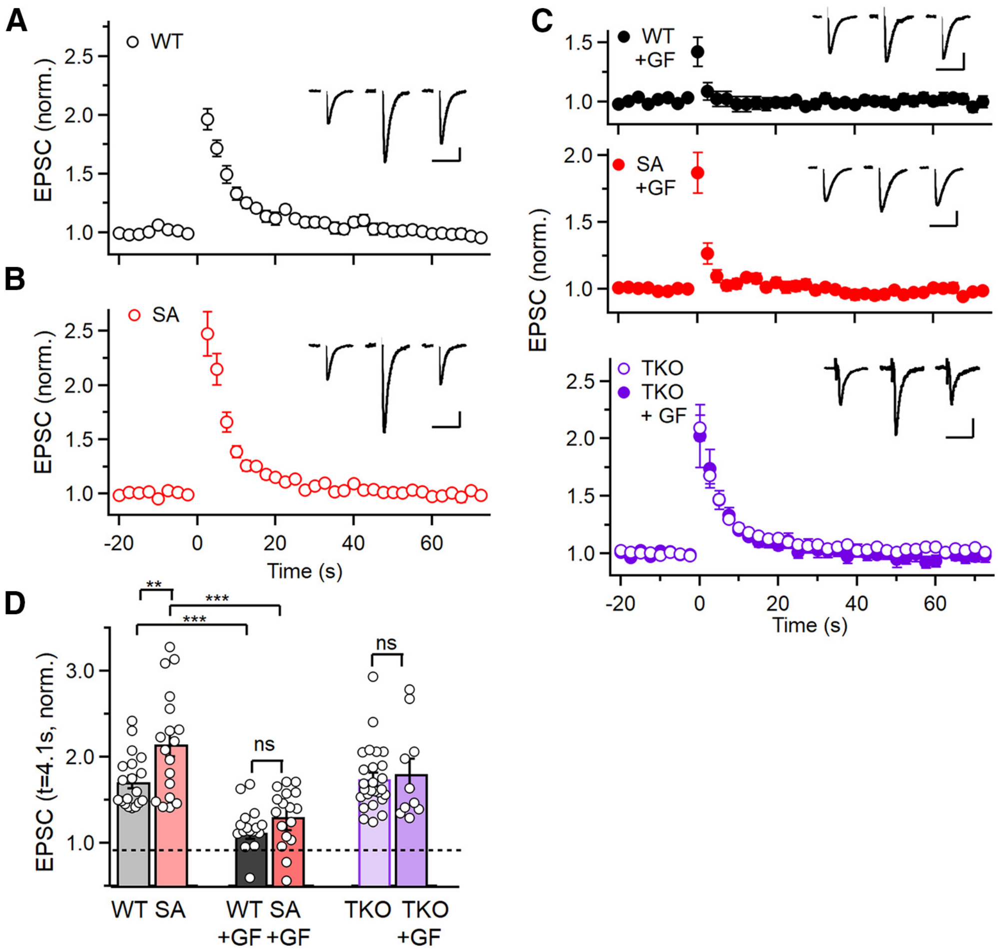

Figure 5. At PF-to-PC synapses, most PKC-dependent PTP does not rely on Munc18-1 phosphorylation. PTP evoked by 10 stimuli at 50 Hz was examined at the granule cell-to-Purkinje cell synapse. ***A***, Wild-type animals in control conditions (open black symbols). Inset, Example EPSCs recorded at −2.5, 4.1, and 60 s. Calibration: 200 pA, 20 ms. ***B***, PTP in Munc18-1SA mice. ***C***, The effect of 10 stimuli at 50 Hz on EPSC amplitude in the presence of the broad-spectrum PKC inhibitor GF (solid symbols) is shown for WT, SA, and PKC$\alpha\beta\gamma$ TKO mice. Insets, EPSCs recorded in the presence of GF. PTP induced in PKC$\alpha\beta\gamma$ TKO mice in control conditions is included for comparison. ***D***, Summary of effects of 10 stimuli at 50 Hz on EPSC amplitude for the indicated conditions. The second point after tetanic stimulation is plotted to reduce the effects of short-lived plasticity that persist in the presence of GF. See Table 4.

Table 4. Data summary for Figure 5 Magnitude of PTP at granule cell PF-to-PC synapse data summary ($t = 4.1$ s)

	WT	SA	WT vs SA	WT (GF)	SA (GF)	WT vs SA (GF)	TKO	TKO (GF)	TKO vs TKO (GF)
PTP	1.717 ± 0.71 ($n = 19$; $N = 8$)	2.146 ± 0.145 ($n = 18$, $N = 8$)	$p = 0.02$	1.089 ± 0.074 ($n = 17$ $N = 8$)	1.265 ± 0.076 ($n = 17$, $N = 7$)	$p = 0.8$	1.677 ± 0.0689 ($n = 26$, $N = 8$)	1.738 ± 0.166 ($n = 10$, $N = 3$)	$p = 0.9$

WT versus WT (GF), $p = 0.0002$; SA versus SA (GF), $p < 0.0001$. p Values were obtained using two-way ANOVA and Tukey's multiple-comparisons test.

a variable contribution to PTP at different synapses, and that this mechanism is not a universal mechanism responsible for the bulk of PTP at most synapses.

PKC phosphorylation of Munc18-1 and enhancement by phorbol esters

There are also differences in the contribution of Munc18-1 phosphorylation to enhancement by phorbol esters at different synapses. Here, in Munc18-1SA mice the phorbol ester enhancement of evoked synaptic responses was not significantly different at the CA3-to-CA1 synapse (despite a trend toward reduced enhancement; Fig. 3*A*) and was essentially unchanged at the PF-to-PC synapse (Fig. 3*B*). This compares to complete elimination in cultured hippocampal synapses (Wierda et al., 2007) and a reduction by ~50% at the calyx of Held (Genç et al., 2014) for a similar manipulation. The phorbol ester enhancement of mEPSC frequency was reduced by ~10% at the CA3-to-CA1 synapse (Fig. 3*C*), was increased at PF-to-PC synapses (Fig. 3*D*), was completely eliminated in cultured hippocampal synapses (Wierda et al., 2007; Genç et al., 2014), and was reduced by ~50% at the calyx of Held (Genç et al., 2014). Thus, just as with PTP, the contribution of PKC phosphorylation of Munc18-1 to phorbol ester-mediated enhancement of transmission is highly synapse dependent.

Challenges in determining the behavioral roles of PTP

It has been extremely difficult to determine the behavioral roles of PTP and other forms of short-term plasticity. This requires a means of selectively eliminating PTP, and ideally targeting specific types of synapses. Some of the challenges are apparent in considering PTP at hippocampal and cerebellar synapses. The implication of PKC in PTP suggested a target, but with PKC involved in many aspects of cell signaling more specificity is needed. The possibility that PTP is mediated by PKC phosphorylation of Munc18-1 suggested that replacing Munc18-1 with Munc18-1SA could provide a means of selectively perturbing PTP. However, our studies have established that PTP is not eliminated at these synapses in Munc18-1SA mice, and that these mice are not suitable for determining the behavioral role of PTP.

References

Abeliovich A, Paylor R, Chen C, Kim JJ, Wehner JM, Tonegawa S (1993) PKCγ mutant mice exhibit mild deficits in spatial and contextual learning. Cell 75:1263–1271.

Alle H, Jonas P, Geiger JR (2001) PTP and LTP at a hippocampal mossy fiber-interneuron synapse. Proc Natl Acad Sci U S A 98:14708–14713.

Arunachalam L, Han L, Tassew NG, He Y, Wang L, Xie L, Fujita Y, Kwan E, Davletov B, Monnier PP, Gaisano HY, Sugita S (2008) Munc18-1 is critical for plasma membrane localization of syntaxin1 but not of SNAP-25 in PC12 cells. Mol Biol Cell 19:722–734.

Beierlein M, Fioravante D, Regehr WG (2007) Differential expression of posttetanic potentiation and retrograde signaling mediate target-dependent short-term synaptic plasticity. Neuron 54:949–959.

Brager DH, Cai X, Thompson SM (2003) Activity-dependent activation of presynaptic protein kinase C mediates post-tetanic potentiation. Nat Neurosci 6:551–552.

Broeke JH, Roelandse M, Luteijn MJ, Boiko T, Matus A, Toonen RF, Verhage M (2010) Munc18 and Munc13 regulate early neurite outgrowth. Biol Cell 102:479–488.

Brose N, Rosenmund C (2002) Move over protein kinase C, you've got company: alternative cellular effectors of diacylglycerol and phorbol esters. J Cell Sci 115:4399–4411.

Chapman PF, Frenguelli BG, Smith A, Chen CM, Silva AJ (1995) The α-Ca2+/calmodulin kinase II: a bidirectional modulator of presynaptic plasticity. Neuron 14:591–597.

Craig TJ, Evans GJ, Morgan A (2003) Physiological regulation of Munc18/nSec1 phosphorylation on serine-313. J Neurochem 86:1450–1457.

Dawidowski D, Cafiso DS (2013) Allosteric control of syntaxin 1a by Munc18-1: characterization of the open and closed conformations of syntaxin. Biophys J 104:1585–1594.

Dawidowski D, Cafiso DS (2016) Munc18-1 and the syntaxin-1 N terminus regulate open-closed states in a t-SNARE complex. Structure 24:392–400.

de Jong AP, Fioravante D (2014) Translating neuronal activity at the synapse: presynaptic calcium sensors in short-term plasticity. Front Cell Neurosci 8:356.

de Jong APH, Meijer M, Saarloos I, Cornelisse LN, Toonen RFG, Sørensen JB, Verhage M (2016) Phosphorylation of synaptotagmin-1 controls a post-priming step in PKC-dependent presynaptic plasticity. Proc Natl Acad Sci U S A 113:5095–5100.

de Vries KJ, Geijtenbeek A, Brian EC, de Graan PN, Ghijsen WE, Verhage M (2000) Dynamics of Munc18-1 phosphorylation/dephosphorylation in rat brain nerve terminals. Eur J Neurosci 12:385–390.

Dingledine R, Somjen G (1981) Calcium dependence of synaptic transmission in the hippocampal slice. Brain Res 207:218–222.

Dulubova I, Sugita S, Hill S, Hosaka M, Fernandez I, Südhof TC, Rizo J (1999) A conformational switch in syntaxin during exocytosis: role of Munc18. EMBO J 18:4372–4382.

Dymecki SM (1996) Flp recombinase promotes site-specific DNA recombination in embryonic stem cells and transgenic mice. Proc Natl Acad Sci U S A 93:6191–6196.

Emperador-Melero J, Wong MY, Wang SSH, de Nola G, Nyitrai H, Kirchhausen T, Kaeser PS (2021) Phosphorylation triggers presynaptic phase separation of Liprin-α3 to control active zone structure. Nat Commun 12:3057.

Fioravante D, Chu Y, Myoga MH, Leitges M, Regehr WG (2011) Calcium-dependent isoforms of protein kinase C mediate posttetanic potentiation at the calyx of Held. Neuron 70:1005–1019.

Fioravante D, Myoga MH, Leitges M, Regehr WG (2012) Adaptive regulation maintains posttetanic potentiation at cerebellar granule cell synapses in the absence of calcium-dependent PKC. J Neurosci 32:13004–13009.

Fiumara F, Milanese C, Corradi A, Giovedì S, Leitinger G, Menegon A, Montarolo PG, Benfenati F, Ghirardi M (2007) Phosphorylation of synapsin domain A is required for post-tetanic potentiation. J Cell Sci 120:3228–3237.

Genç Ö, Kochubey O, Toonen RF, Verhage M, Schneggenburger R (2014) Munc18-1 is a dynamically regulated PKC target during short-term enhancement of transmitter release. Elife 3:e01715.

Han GA, Malintan NT, Collins BM, Meunier FA, Sugita S (2010) Munc18-1 as a key regulator of neurosecretion. J Neurochem 115:1–10.

Hori T, Takai Y, Takahashi T (1999) Presynaptic mechanism for phorbol ester-induced synaptic potentiation. J Neurosci 19:7262–7267.

Imig C, Min SW, Krinner S, Arancillo M, Rosenmund C, Südhof TC, Rhee J, Brose N, Cooper BH (2014) The morphological and molecular nature of synaptic vesicle priming at presynaptic active zones. Neuron 84:416–431.

Jackman SL, Turecek J, Belinsky JE, Regehr WG (2016) The calcium sensor synaptotagmin 7 is required for synaptic facilitation. Nature 529:88–91.

Junge HJ, Rhee JS, Jahn O, Varoqueaux F, Spiess J, Waxham MN, Rosenmund C, Brose N (2004) Calmodulin and Munc13 form a Ca2+ sensor/effector complex that controls short-term synaptic plasticity. Cell 118:389–401.

Kohansal-Nodehi M, Chua JJ, Urlaub H, Jahn R, Czernik D (2016) Analysis of protein phosphorylation in nerve terminal reveals extensive changes in active zone proteins upon exocytosis. Elife 5:e14530.

Korogod N, Lou X, Schneggenburger R (2007) Posttetanic potentiation critically depends on an enhanced Ca(2+) sensitivity of vesicle fusion mediated by presynaptic PKC. Proc Natl Acad Sci U S A 104:15923–15928.

Lee D, Lee KH, Ho WK, Lee SH (2007) Target cell-specific involvement of presynaptic mitochondria in post-tetanic potentiation at hippocampal mossy fiber synapses. J Neurosci 27:13603–13613.

Lee JS, Kim MH, Ho WK, Lee SH (2008) Presynaptic release probability and readily releasable pool size are regulated by two independent mechanisms during posttetanic potentiation at the calyx of Held synapse. J Neurosci 28:7945–7953.

Leitges M, Schmedt C, Guinamard R, Davoust J, Schaal S, Stabel S, Tarakhovsky A (1996) Immunodeficiency in protein kinase cbeta-deficient mice. Science 273:788–791.

Leitges M, Plomann M, Standaert ML, Bandyopadhyay G, Sajan MP, Kanoh Y, Farese RV, Letiges M (2002) Knockout of PKC alpha enhances insulin signaling through PI3K. Mol Endocrinol 16:847–858.

Lewandoski M, Martin GR (1997) Cre-mediated chromosome loss in mice. Nat Genet 17:223–225.

Lou X, Scheuss V, Schneggenburger R (2005) Allosteric modulation of the presynaptic Ca2+ sensor for vesicle fusion. Nature 435:497–501.

Lou X, Korogod N, Brose N, Schneggenburger R (2008) Phorbol esters modulate spontaneous and Ca^{2+}-evoked transmitter release via acting on both Munc13 and protein kinase C. J Neurosci 28:8257–8267.

Malenka RC, Madison DV, Nicoll RA (1986) Potentiation of synaptic transmission in the hippocampus by phorbol esters. Nature 321:175–177.

Nielander HB, Onofri F, Valtorta F, Schiavo G, Montecucco C, Greengard P, Benfenati F (1995) Phosphorylation of VAMP/synaptobrevin in synaptic vesicles by endogenous protein kinases. J Neurochem 65:1712–1720.

Rhee J-S, Betz A, Pyott S, Reim K, Varoqueaux F, Augustin I, Hesse D, Südhof TC, Takahashi M, Rosenmund C, Brose N (2002) β phorbol ester- and diacylglycerol-induced augmentation of transmitter release is mediated by Munc13s and not by PKCs. Cell 108:121–133.

Rizo J (2018) Mechanism of neurotransmitter release coming into focus. Protein Sci 27:1364–1391.

Rosahl TW, Spillane D, Missler M, Herz J, Selig DK, Wolff JR, Hammer RE, Malenka RC, Südhof TC (1995) Essential functions of synapsins I and II in synaptic vesicle regulation. Nature 375:488–493.

Saitoh N, Hori T, Takahashi T (2001) Activation of the epsilon isoform of protein kinase C in the mammalian nerve terminal. Proc Natl Acad Sci U S A 98:14017–14021.

Shapira R, Silberberg SD, Ginsburg S, Rahamimoff R (1987) Activation of protein kinase C augments evoked transmitter release. Nature 325:58–60.

Shimazaki Y, Nishiki T, Omori A, Sekiguchi M, Kamata Y, Kozaki S, Takahashi M (1996) Phosphorylation of 25-kDa synaptosome-associated protein. Possible involvement in protein kinase C-mediated regulation of neurotransmitter release. J Biol Chem 271:14548–14553.

Toonen RFG, De Vries KJ, Zalm R, Südhof TC, Verhage M (2005) Munc18-1 stabilizes syntaxin 1, but is not essential for syntaxin 1 targeting and SNARE complex formation. J Neurochem 93:1393–1400.

Vandael D, Borges-Merjane C, Zhang X, Jonas P (2020) Short-term plasticity at hippocampal mossy fiber synapses is induced by natural activity patterns and associated with vesicle pool engram formation. Neuron 107:509–521.e7.

Verhage M, Maia AS, Plomp JJ, Brussaard AB, Heeroma JH, Vermeer H, Toonen RF, Hammer RE, van den Berg TK, Missler M, Geuze HJ, Südhof TC (2000) Synaptic assembly of the brain in the absence of neurotransmitter secretion. Science 287:864–869.

Vyleta NP, Borges-Merjane C, Jonas P (2016) Plasticity-dependent, full detonation at hippocampal mossy fiber-CA3 pyramidal neuron synapses. Biochem Pharmacol 5:e17977.

Wang CC, Weyrer C, Paturu M, Fioravante D, Regehr WG (2016) Calcium-dependent protein kinase C is not required for post-tetanic potentiation at the hippocampal CA3 to CA1 synapse. J Neurosci 36:6393–6402.

Wang D, Maler L (1998) Differential roles of Ca2+/calmodulin-dependent kinases in posttetanic potentiation at input selective glutamatergic pathways. Proc Natl Acad Sci U S A 95:7133–7138.

Weyrer C, Turecek J, Niday Z, Liu PW, Nanou E, Catterall WA, Bean BP, Regehr WG (2019) The Role of Ca_V2.1 channel facilitation in synaptic facilitation. Cell Rep 26:2289–2297.e3.

Wierda KD, Toonen RF, de Wit H, Brussaard AB, Verhage M (2007) Interdependence of PKC-dependent and PKC-independent pathways for presynaptic plasticity. Neuron 54:275–290.

Zeng L, Webster SV, Newton PM (2012) The biology of protein kinase C. Adv Exp Med Biol 740:639–661.

Zucker RS, Regehr WG (2002) Short-term synaptic plasticity. Annu Rev Physiol 64:355–405.